# Portable Marx Generator for Microplasma Applications

T. UENO\*, T. SAKUGAWA\*\*, M. AKIYAMA\*\*, T. NAMIHIRA\*\*, S. KATSUKI\*\*
and H. AKIYAMA\*\*

*\*Department of Electrical and Electronics Engineering, Oita*

*National College of Technology, Maki 1666, Oita 870-0152, Japan*

*\*\*Graduate School of Science and Technology, Kumamoto University,*

*Kurokami 1-39-1, Kumamoto 860-8555, Japan*

There are many applications using pulsed power such as the triggering of high speed cameras and spectrometers, the processing or chemical analysis of minute material, and the stimulation of cells by electrical pulses. The pulse width and voltage required for each application are different in the range of ns and kV. The energy required is usually in the mJ regime. Here, a novel portable pulse power generator with 35 ns pulse width and 2.5 kV output voltage has been developed, and applied to the microplasma production. The solid-state switches are used for the high speed closing. The advantages of solid-state switches are compactness, reliability, stability of the breakdown voltage, and lifetime in comparison with those using discharges. The key point to achieve the fast risetime is to use the avalanche breakdown of the bipolar junction transistors (BJTs). The behavior of the basic switching circuit using BJTs in avalanche mode is described, and also the developed pulsed power generator is applied to produce the microplasma.

Keywords: Marx generator, Avalanche breakdown, Microplasma, Pulsed Power

## 1. Introduction

The microplasma jet has been used in various fields such as materials processing, chemical analysis, short-wavelength light source, and biomaterials treatment [1, 2]. The miniaturized electric power generator has been requested to produce these plasmas in the micro-scale area, because the present large size generator limits the use of these small plasmas [3]. Under such background, a miniaturized Marx generator which has Bipolar Junction Transistors (BJTs) as closing switches has been developed to generate microplasma jet [4]. In the miniaturized Marx generator, BJTs were operated in avalanche mode to obtain a faster switching speed with nanoseconds regime.

In this paper, three kinds of BJTs which have the different collector currents are evaluated as closing switch, and the microplasma jet is generated by the miniaturized Marx generator. The generator is able to output -2.5kV, 38ns pulse-width by series BJTs for cutting load current. It has been found that the length of microplasma jet was depended on load current.

## 2. Marx generator

In the conventional Marx generator, the pulse rise time is mainly limited due to the speed of the switches and the stray inductance. After the switches turn on, the circuit is modeled as a simple *RLC* circuit, where a charged capacitor is discharged through a *RL* series connection [5]. The effective capacitance $C$ is $C = C_{stage} / N$, where $C_{stage}$ and $N$ are the stage capacitance and the number of stages, respectively. Inductance $L$ and resistance $R$ are lumped from all sources and include the load inductance and resistance. In the case that the circuit resistance $R$ is smaller than $R < 2 \times (L/C)^{-0.5}$ the rise time is dominated by the oscillatory frequency and may be approximated by $t_{ru} = 1.2 \times (L \times C)^{0.5}$. In the critically damped case where $R = 2 \times (L/C)^{-0.5}$ the rise time is given by $t_{rc} = 2 \times L/R$, and in the over damped case where $R > 2 \times (L/C)^{-0.5}$ the rise time is dominated by the inductance and can be approximated with $t_{ro} = 2.3 \times L/R$. In the case that rise time is critical the over damped case is preferable, since $t_{ro} < t_{rc} < t_{ru}$. In any cases, the inductance of the system should be minimized to reduce the rise time. The discussion above neglects the switching transition and assumes that the switch works instantaneously, and frequently the transition itself would determine the current rise time into the load.

## 3. Avalanche breakdown

The avalanche breakdown occurs when the collector to emitter voltage is over a breakdown voltage. It is difficult to characterize the breakdown voltage from the typical datasheets. In this chapter, the BJTs as switching

ueno@oita-ct.ac.jp

device of the miniaturized Marx generator are evaluated.

Figure 1 shows the evaluation circuit of BJT switching. The circuit is consisted of a charging resistor ($R_{ch}$=20 kΩ), a BJT, a capacitor and TTL signal generator. In this work, three BJTs, named 2SC2655, 2SC5076 and 2SC5000 (NPN type Bipolar Junction Transistor, Toshiba, Japan), are evaluated as a closing switch. The maximum voltage between collector and emitter, $V_{CEO}$ of three BJTs on the data sheets, is 50V. The maximum collector currents, $I_{co}$ of 2SC2655, 2SC5076 and 2SC5000 BJTs, are 2A, 5A and 10 A, respectively. For the evaluation of BJTs, the capacitance is changed from 0.015μF to 1.0 μF. The capacitor is charged till $V_{ch}$ through the charging resistor. The TTL signal from generator (33220A, Agilent) is applied between the base and the emitter of BJT at 3 pps (pulses per second). The voltage between collector and emitter, $V_c$, and the collector current, $I_c$, are measured by the high voltage probe (PHV641, PMK) and the current transformer (Model 2877, Pearson Electronics) which is located on the emitter of BJT, respectively. The signals are recorded by the digital storage oscilloscope (TDS3034B, Tektronix).
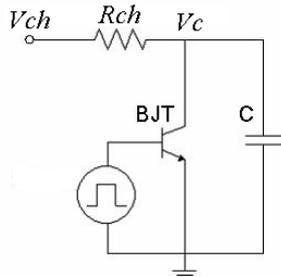


Fig.1 Evaluation circuit of BJT.

## 3-1. Leakage current in avalanche breakdown

Figure 2 is the dependence of $V_c$ on $V_{ch}$ in the case of using 2SC2655 BJT. The $V_c$ increases linearly with $V_{ch}$ in the range of 0 to 160 V. Over 170 V of $V_{ch}$, $V_c$ is less than $V_{ch}$. The leakage current in the evaluation circuit appears when $V_{ch}$ reaches 170V. In the case of other BJTs (2SC5076 and 2SC5000), the onset voltage of the leakage current is 200V. From these results, the further evaluations of BJTs are carried out in the range from 0 to the onset voltage of leakage current.
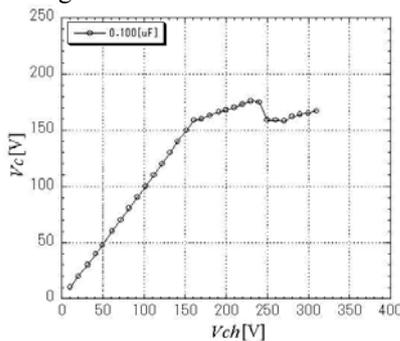


Fig.2 Dependence of $V_c$ on $V_{ch}$ (2SC2655).

## 3-2.Switching voltage and current waveforms

Figure 3 shows the typical $V_c$ and $I_c$ waveforms in the case of using 2SC2655 BJT and 0.1 μF of the capacitor. Figure 3 (a) shows the waveforms in the operation with 50 V of $V_{ch}$. On the other hand, Figure 3 (b) indicates the waveforms in the operation with 140 V of $V_{ch}$. It is observed from Figure 3 (a) that the $V_c$ falls down from 50 to 0 within 500 ns. The peak of $I_c$ is limited lower than 6 A, which is 3 times of specified current. Here, it is noted that the switching time is defined as the time duration of the voltage fall time from 90 % to 10 % of $V_{ch}$. From Figure 3 (a), the switching time of 2SC2655 BJT is 500 ns. From Figure 3 (b), the $V_c$ falls down from 140 to 0 within 150 ns. The peak of $I_c$ is 90 A which is 45 times of specified current. The switching time of 2SC2655 BJT is 120 ns.

Figure 4 shows the waveforms of $I_c$ in the case of using 2SC5000 BJT and 0.1μF of the capacitor for three different $V_{ch}$. It is shown from Figure 4 that the operation mode of BJT shifts from the normal mode to the avalanche mode when $I_c$ exceeds the threshold current. This threshold current is about 3 times of specified current. This threshold current is different depending on the $V_{ch}$. As $V_{ch}$ increases, the rise time of $I_c$ becomes faster, therefore $I_c$ exceeds the threshold at the earlier time.
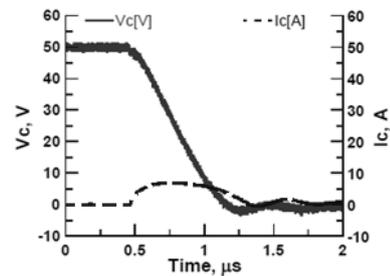


(a) When BJT is operated in normal mode.
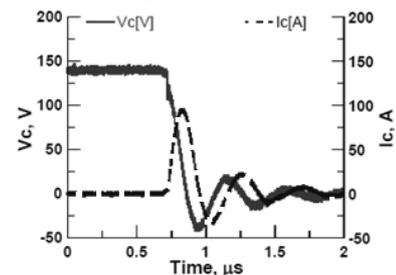


(b) When BJT is operated in avalanche mode.

Fig.3 Waveforms of $V_c$ and $I_c$.
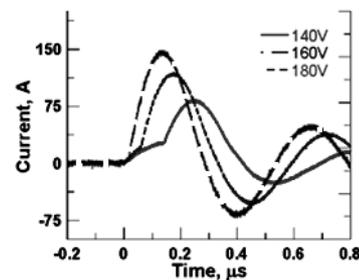


Fig.4 Collector current waveforms for three different $V_{ch}$. (2SC5000, $C$=0.100uF).

## 3-3. Current and voltage characteristics in avalanche breakdown

Figure 5 shows the current and voltage characteristics in the case of using 2SC2655 BJT. In normal mode operation, $I_c$ is limited by the specification current. In the avalanche mode operation, $I_c$ increases faster and reaches the value, which is given by

$$I_c = V_c \sqrt{\frac{C}{L_c}}, \qquad (1)$$

where $C$ and $L$ are the capacitance and circuit inductance, respectively. This relational expression is clear from Figure 5, since $I_c$ is proportional to $V_c$ or square root $C$ in the avalanche mode operation.

Figure 6 shows the comparison of the current and voltage characteristics for different BJT. When BJT is operated in normal mode operation, $I_c$ of each BJT has the 5 times difference. However, in avalanche mode operation, $I_c$ of each BJT is almost same. Hence, the specification current is not important to use BJT as switching device of the Marx generator.
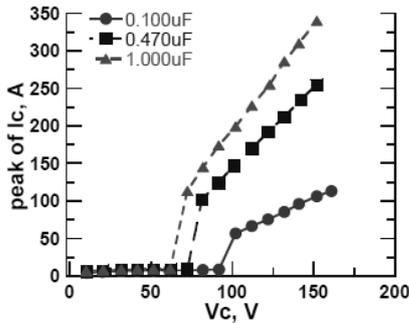


Fig.5 Current and voltage characteristics for different capacitance.
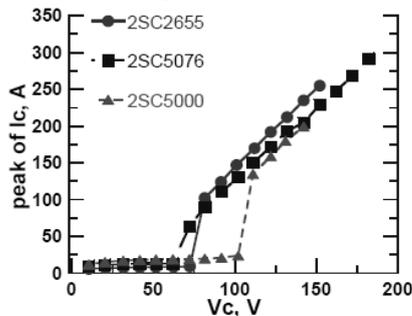


Fig.6 Current and voltage characteristics for different BJTs.

## 3-4. Switching time

Figure 7 shows the dependence of switching time on $V_c$ in the case of using 2SC2655 BJT. In normal mode operation, as $V_c$ or $C$ increase, the switching time increases. In this case, $I_c$ is limited by the specification current. Therefore, when the quantity of electric charge, $Q$, is large, the switching time increases. In the avalanche mode operation, as capacitance increases, the switching time increases. However, the switching time increases as $V_c$ decreases. As discussed previous, $I_c$ exceeds the threshold current in earlier time as the voltage is higher.

Figure 8 shows the dependence of the switching time on $V_c$ for different BJT. The switching time of 2SC2655 is faster than other BJTs, since the specification current is smaller than other BJTs. Hence, the 2SC2655 shifts into avalanche mode faster. In other words, the switching time is faster. The 2SC2655 is suitable as the switching device of the Marx generator.
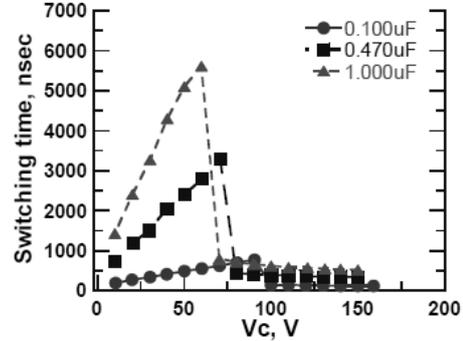


Fig.7 Dependence of switching time on $V_c$ for different capacitance.
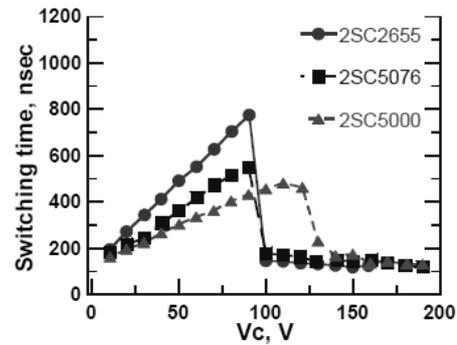


Fig.8 Dependence of switching time on $V_c$ for different BJTs.

## 3-5. Miniaturized Marx generator

The miniaturized Marx generator has been developed using BJT 2SC2655 as switching device. Figure 9 shows the circuit diagram. The circuit is composed of 14 stages, and the capacity of each stage is 0.1 uF. The 14 BJTs are connected in series. The other BJTs placed at the output work in the avalanche mode after a time. Therefore, the waveform of output voltage, that is, the pulse width is constant even though the load is changed.

Figure 10 shows the output waveform at the open circuit load. The charging voltage is 180 V, and the peak output voltage is about -2.5 kV. The FWHM of pulse voltage is about 35 ns. Even though the BJTs are operated at the region over the rating voltage and the rating current, the BJTs work with a long operation of hours for the pulsed mode.
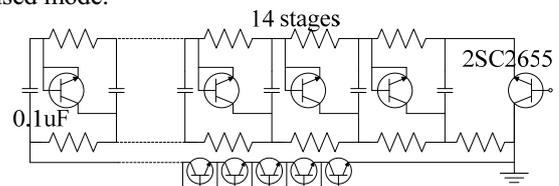


Fig.9 Schematic circuit diagram of Miniaturized Marx generator.
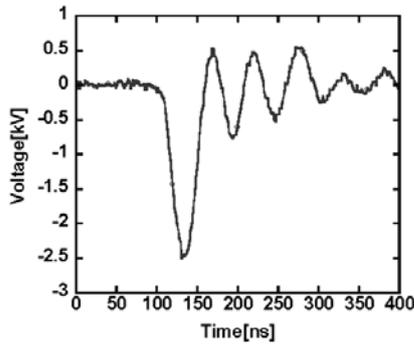
Fig.10 Output voltage of Miniaturized Marx generator.

### 3-6. Microplasma jet

The microplasma jet could be generated by a DC power source and CW sinusoidal power supplies. Our experience shows the problem of heating. Therefore, the pulsed microplasma jet is generated with the developed miniaturized Marx generator. Figure 11 shows the microplasma jet reactor. The reactor electrodes are a tungsten needle and a copper plate. The needle electrode placed in a ceramic tube is the tungsten wire of 0.025mm in diameter. The air of 2.5L/min is flowing through the ceramic tube. The atmospheric plasma is extended from the hole of 1mm in the diameter on copper plate. The camera (D40, Nikon) with 30 seconds of shutter time is used for taking the microplasma jet.

In Figure 12(a), the luminescence from the electrical discharges in the tube and outside of the copper electrode appears. The length of the plasma jet is about 0.5mm when the BJTs placed at the output are operated as a closing switch. On the other hand, the further extension of plasma jet is observed without the series BJTs at the output as shown in Figure 12(b). The length of the plasma jet is about 3mm. Figures 13 and 14 show the voltage and current waveforms with and without the BJTs at the output, respectively. The pulse widths of voltage are different.

The relation between the plasma extension and the input energy into the plasma has been reported in Ref. [6]. Briefly the torch length was closely related to the total volume of plasma.

When the current is supplied into the load continuously, the further extension of plasma jet is observed. The extension of the plasma jet might depend on the input energy into plasma. In addition to the plasma extension, some interesting differences of discharges in the left and right side in Fig. 12 are observed. The discharge colors inside the tube are blue and purple in the left and right side discharges, if Fig.12 is color photographs. Moreover, the discharge between the tube and the electrode is observed only in the right photograph in Fig. 12. The characteristics and the mechanisms of these discharge modes are now unclear and in our future subjects.
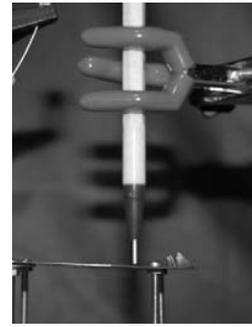


Fig.11 Photograph of microplasma jet reactor.



(a)          (b)
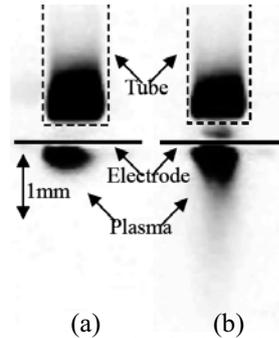
Fig.12 Photograph of microplasma jet.
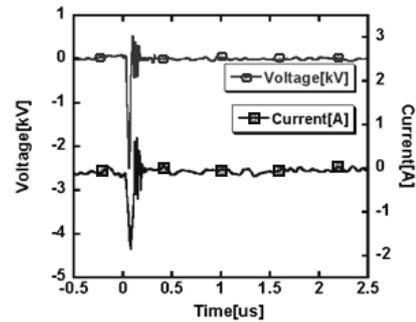


Fig.13 Voltage and current waveforms of microplasma jet reactor with BJTs at output.
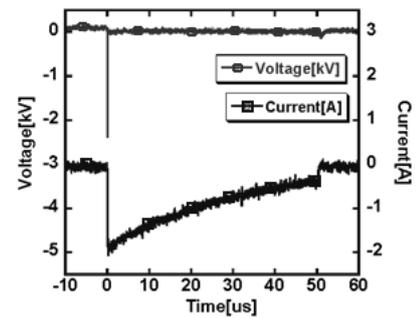


Fig.14 Voltage and current waveforms of microplasma jet reactor without BJTs at output.

### 4. Conclusion

The characteristics of BJTs on the avalanche breakdown was evaluated. The suitable BJT was selected as the switching device for the miniaturized Marx generator. The developed pulsed power generator was applied to produce the microplasma jet.

When the collector current exceeded a threshold

current, the operation mode of BJT shifted from the normal mode to the avalanche mode. It was shown that 2SC2655 was suitable as the switching device of the miniaturized Marx generator from the switching time characteristics. The microplasma jet was successfully generated by the developed miniaturized Marx generator.

[1]  K. Tachibana: Journal of Plasma and Fusion Research, **76**, 435(2000).

[2]  K. Tachibana: Journal of Plasma and Fusion Research, **80**, 825(2004).

[3]  T. Namihira, S. Tsukamoto, D. Wang, S. Katsuki, R. Hackam, K. Okamoto, H. Akiyama: IEEE Transactions on Plasma Science, **28**,109(2000).

[4]  T. Heeren, T. Ueno, D. Wang, T. Namihira, S. Katsuki, H. Akiyama: IEEE Transactions on Plasma Science, **33**, 1205 (2005).

[5]  A. Chatterjee, K. Mallik, S.M. Oak: Review of Scientific Instruments, **69**, 2166(1998).

[6]  C. Jaegu, M. Keita, Y. Hidekazu, S. R. Hosseini, N. Takao; K. Sunao, A. Hidenori: Japanese journal of applied physics, **48**, 016001 (2009).